Dinuclear Lanthanide Complexes supported by a hybrid Salicylaldiminato/ Calix[4]arene-Ligand: Synthesis, Structure, Magnetic and Luminescence Properties of $(HNEt_3)[Ln_2(HL)(L)]$ (Ln = Sm^{III}, Eu^{III}, Gd^{III}, Tb^{III})

Steve Ullmann,[a] Peter Hahn,[a] Laura Blömer,[a] Anne Mehnert,[a] Christian Laube,[c] Bernd Abel,[b,c] and Berthold Kersting[a]*

[a] *Institut für Anorganische Chemie, Universität Leipzig, Johannisallee 29, 04103 Leipzig, Germany,* E-mail: b.kersting@uni-leipzig.de *Fax: +49(0)341-97-36199*

[b] *Leibniz Institute for Surface Engineering (IOM), Department Functional Surfaces, D-04318 Leipzig, Germany*

[c] *Wilhelm-Ostwald-Institut für Physikalische und Theoretische Chemie, Universität Leipzig, Linnéstraße 2, D-04103 Leipzig, Germany*

Supporting Information

Content

1) ORTEP PLOT for $HNEt_3)[Sm_2(HL)(L)(MeCN)_2]\cdot 2.5MeCN$ ($4\cdot 2.5MeCN$).

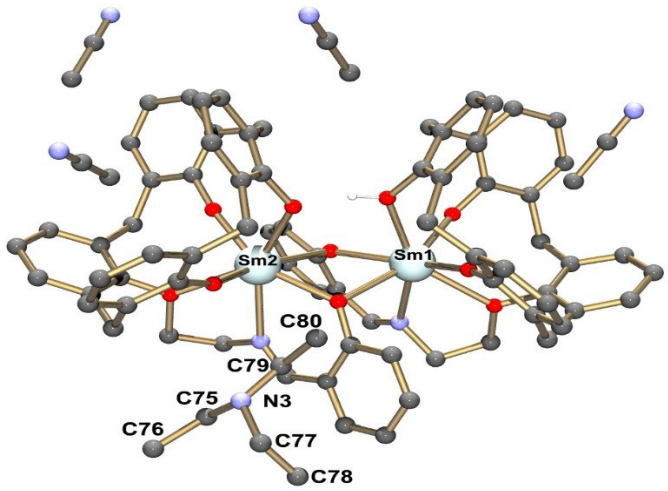

Fig. S1. Single-crystal X-ray diffraction structure of the $[Sm_2(HL)(L)(MeCN)_2]^-$ anion in crystals of $(HNEt_3)[Sm_2(HL)(L)(MeCN)_2]\cdot 2.5MeCN$ (**4**$\cdot 2.5MeCN$). The $HNEt_3^+$ ion and some MeCN solvate molecules are omitted for clarity. Thermal ellipsoids are shown at the 30% probability level.

2. Analytical data for 2

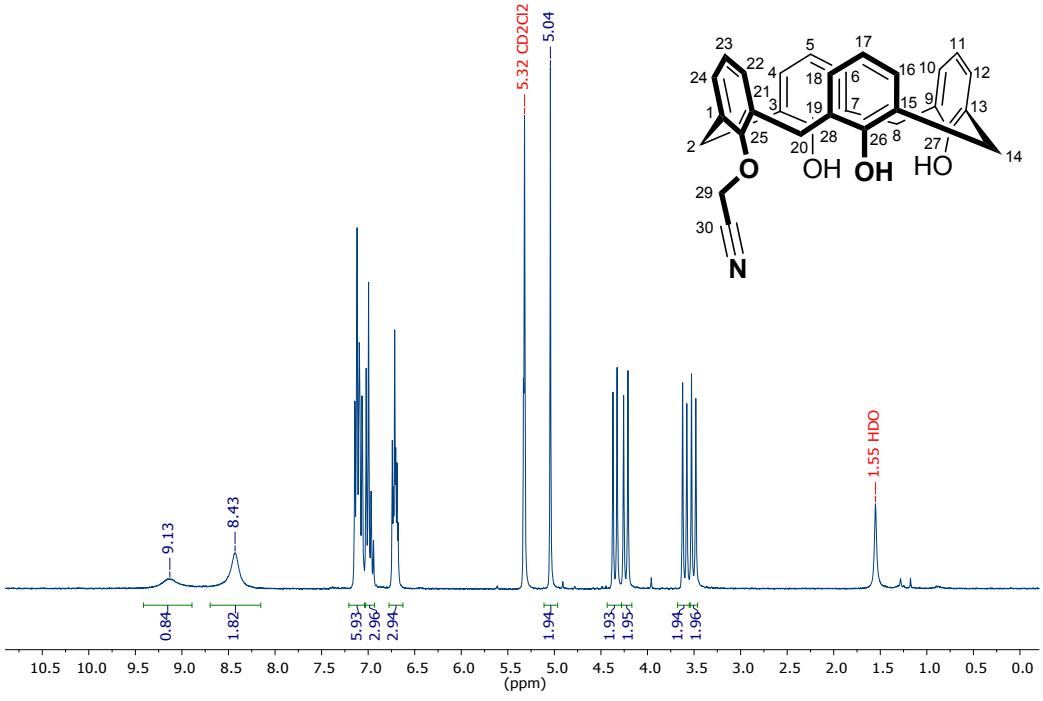

Fig. S2. ^1H NMR spectrum of **2** in CD_2Cl_2 at ambient temperature.

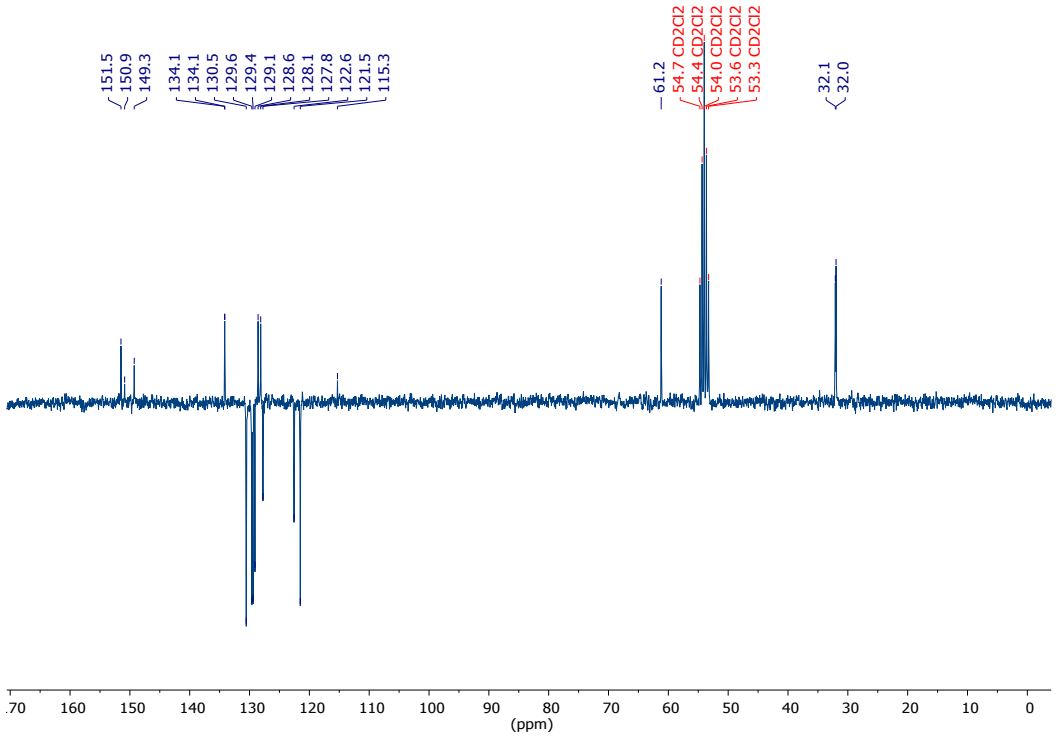

Fig. S3. APT spectrum of **2** in CD_2Cl_2 at ambient temperature.

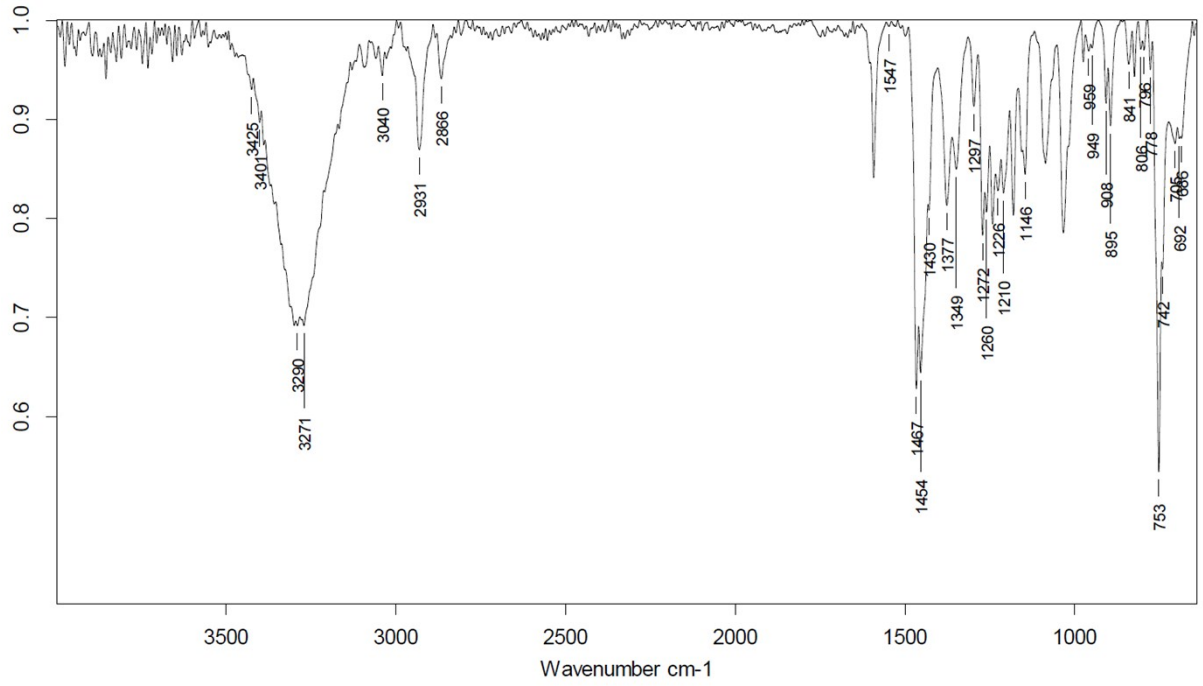

Fig. S4. ATR infrared spectrum of **2**.

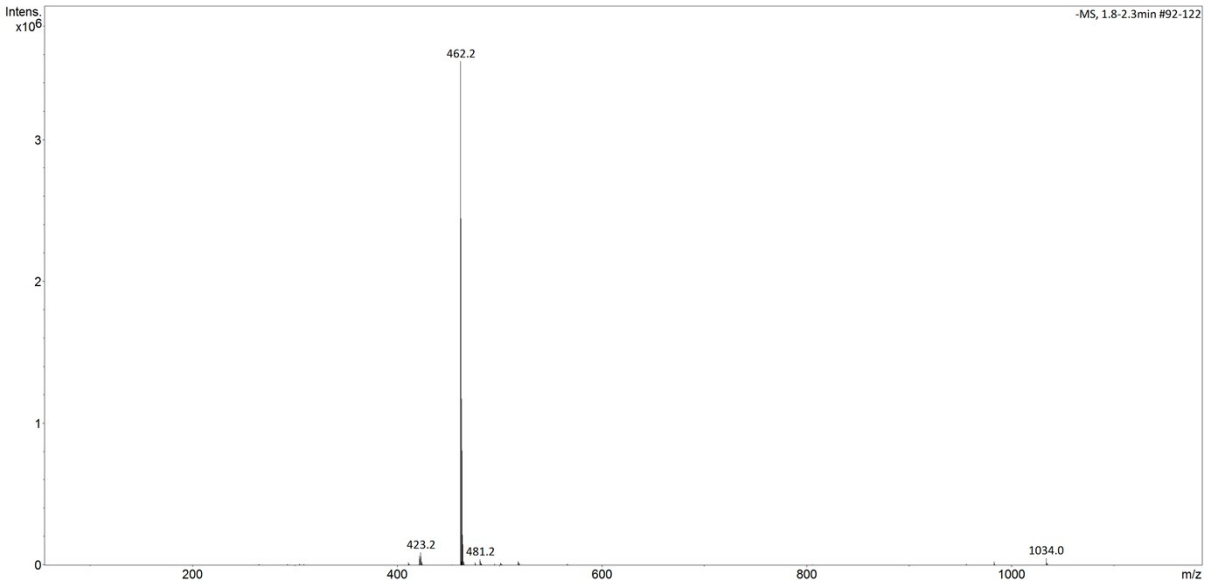

Fig. S5. ESI mass spectrum of **2**.

3. Analytical data for 3

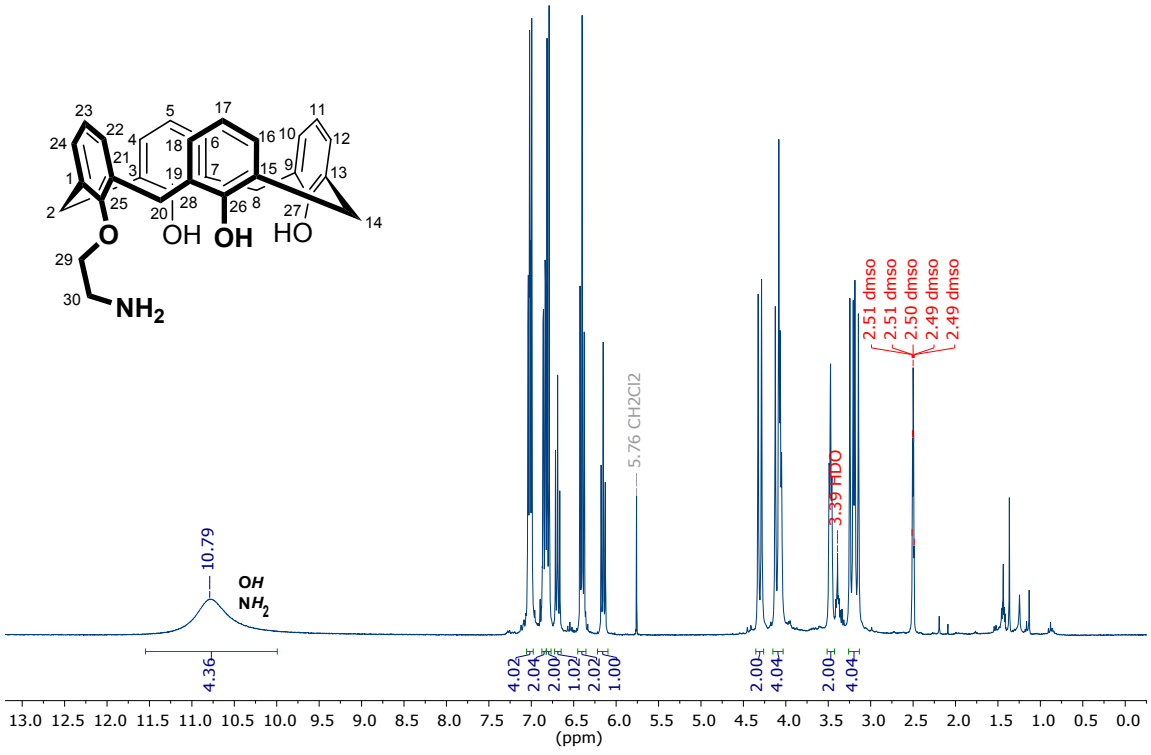

Fig. S6. ^{1}H NMR spectrum of **3** in DMSO-d_6 at ambient temperature.

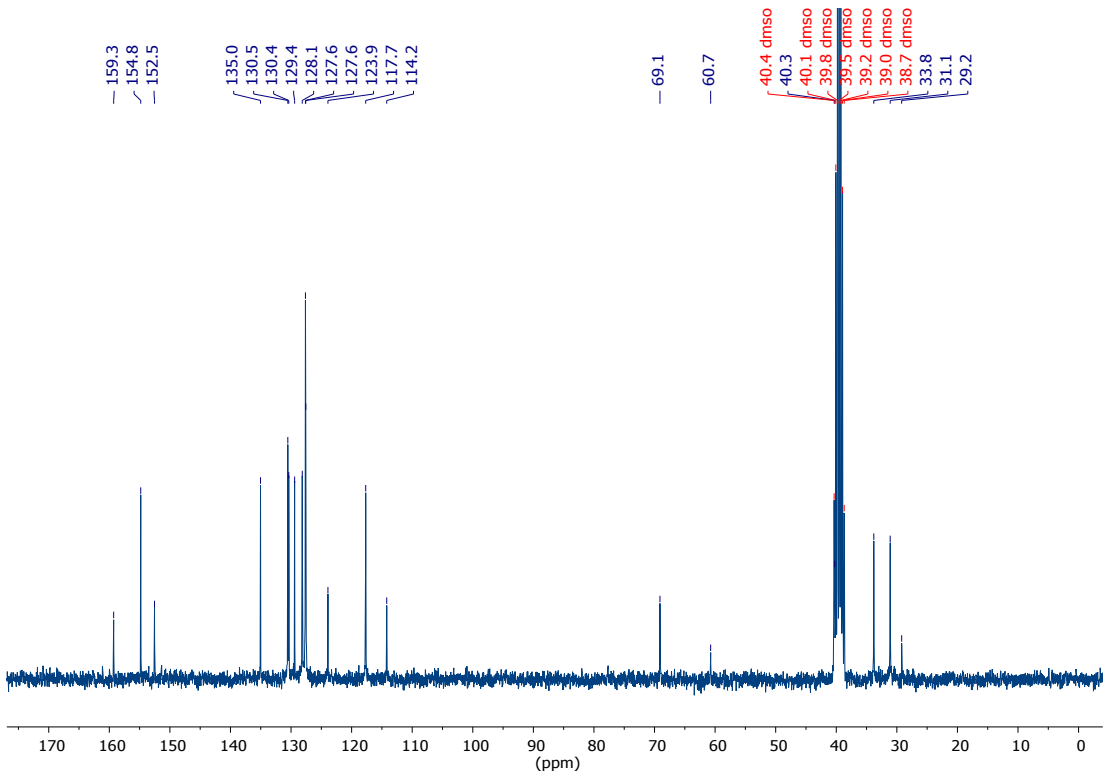

Fig. S7. APT spectrum of **3** in DMSO-d_6 at ambient temperature.

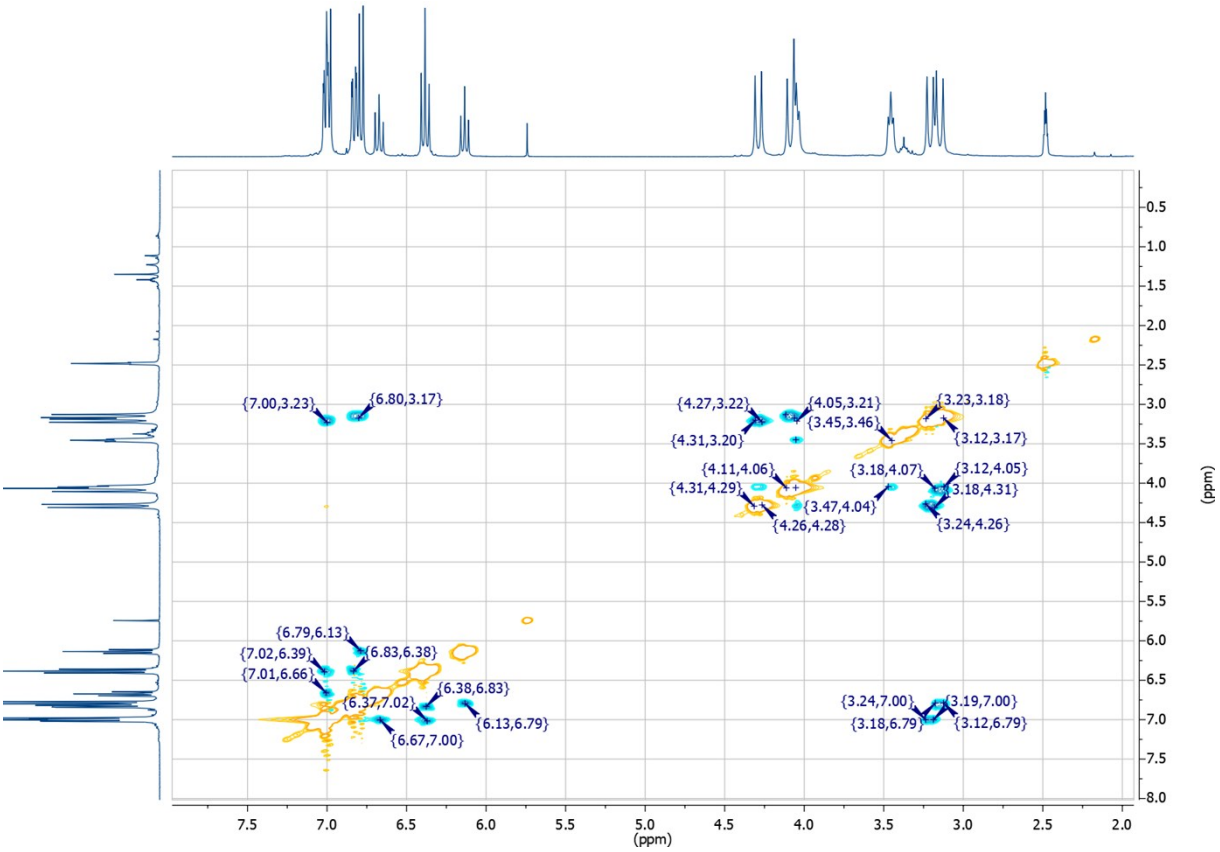

Fig. S8. ^{1}H,^{1}H NOESY spectrum of **3** in DMSO-d_6 at ambient temperature.

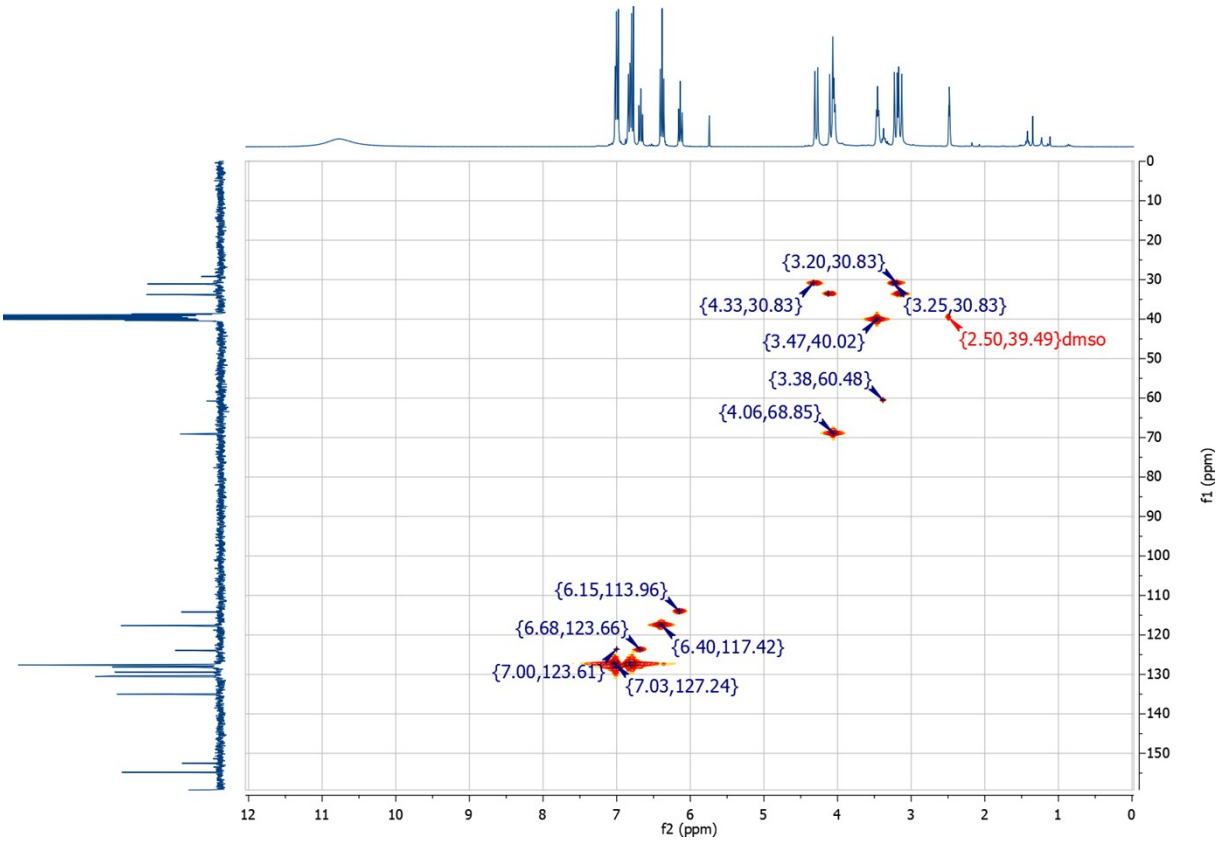

Fig. S9. $^{1}H,^{13}C$ HSQC spectrum of **3** in DMSO-d_6 at ambient temperature.

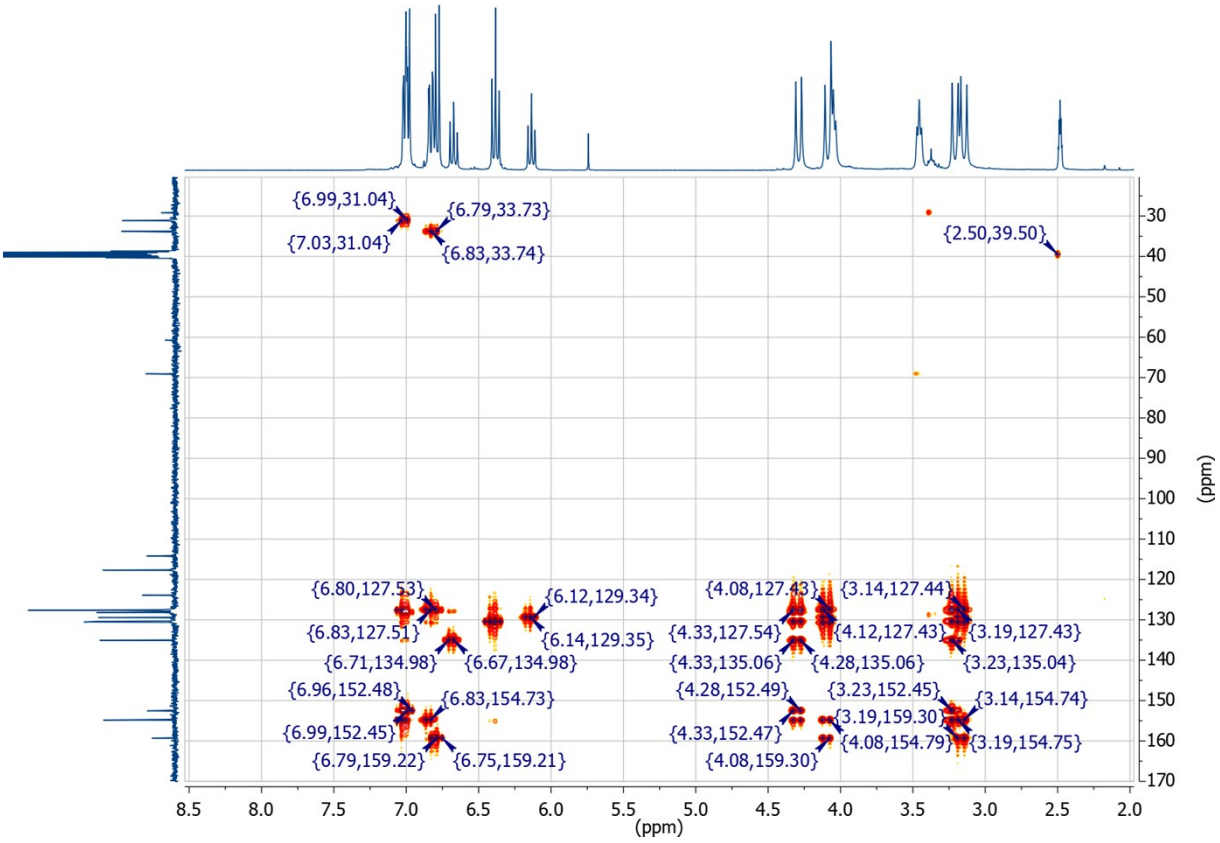

Fig. S10. $^{1}H,^{13}C$ HMBC spectrum of **3** in DMSO-d_6 at ambient temperature.

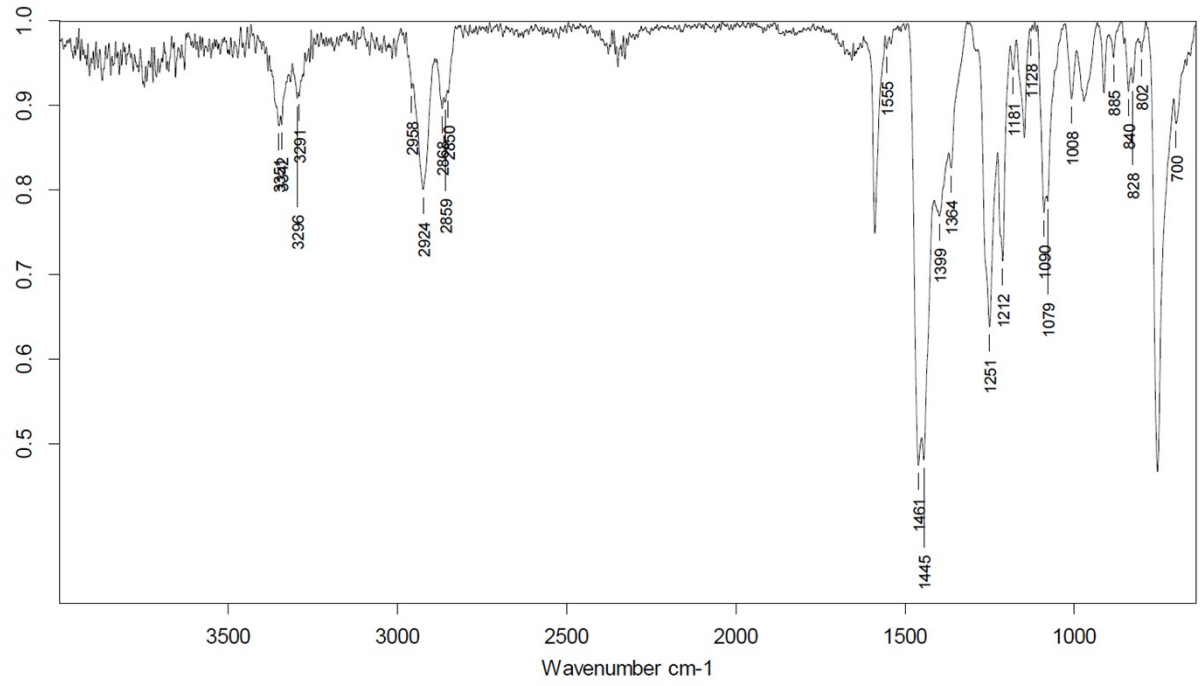

Fig. S11. ATR infrared spectrum of **3**.

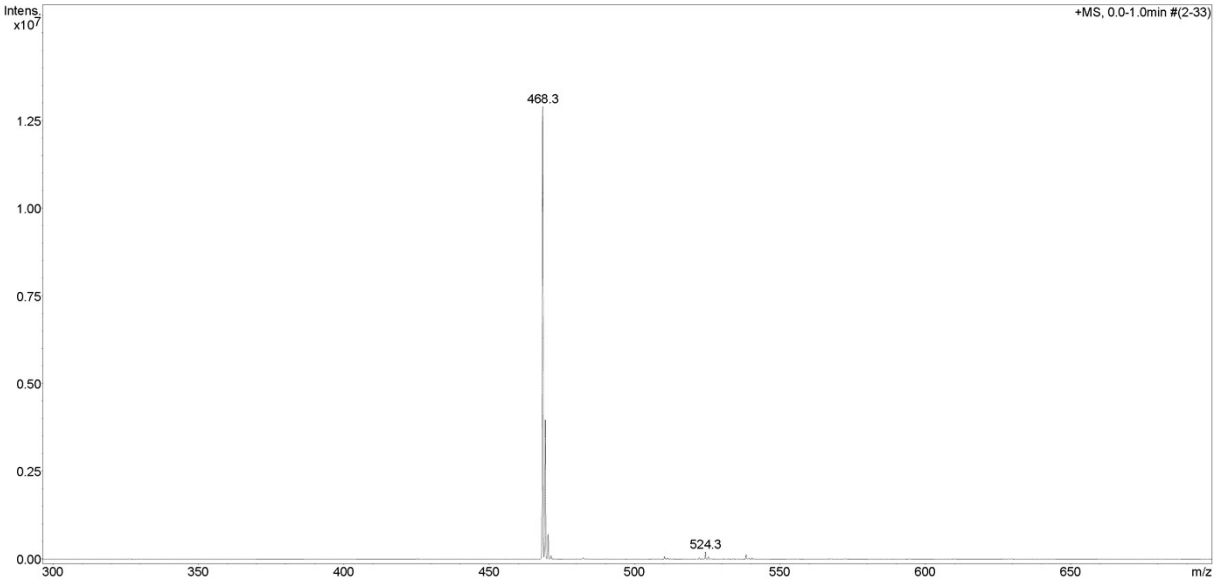

Fig. S12. ESI mass spectrum of **3**.

4. Analytical data for H_4L

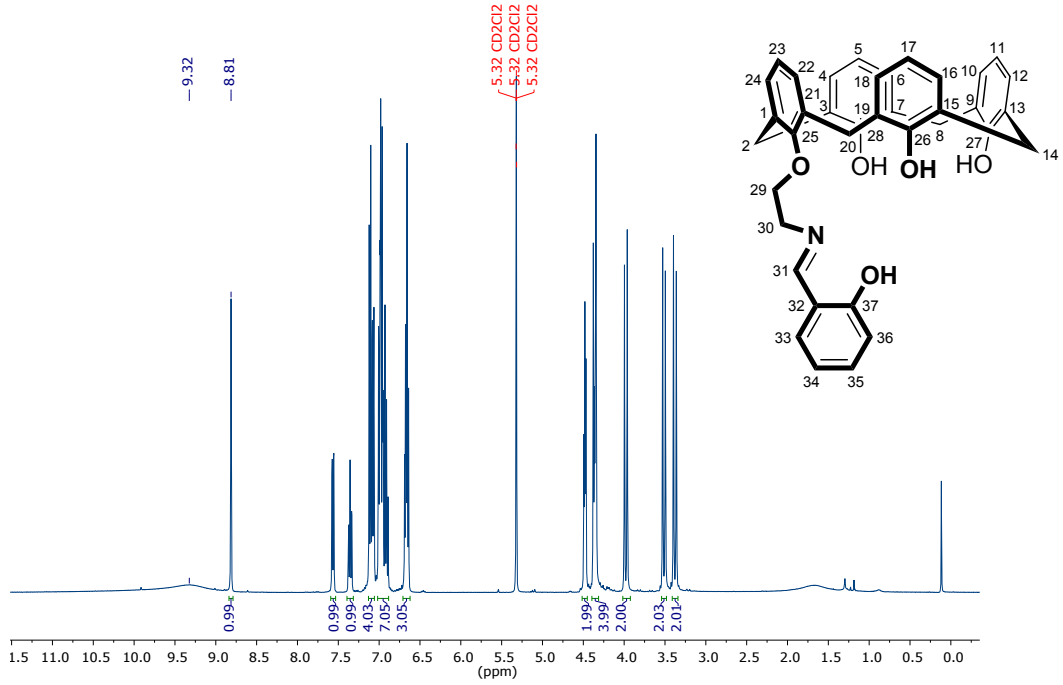

Fig. S13. ^{1}H NMR spectrum of **H_4L** in CD_2Cl_2 at ambient temperature.

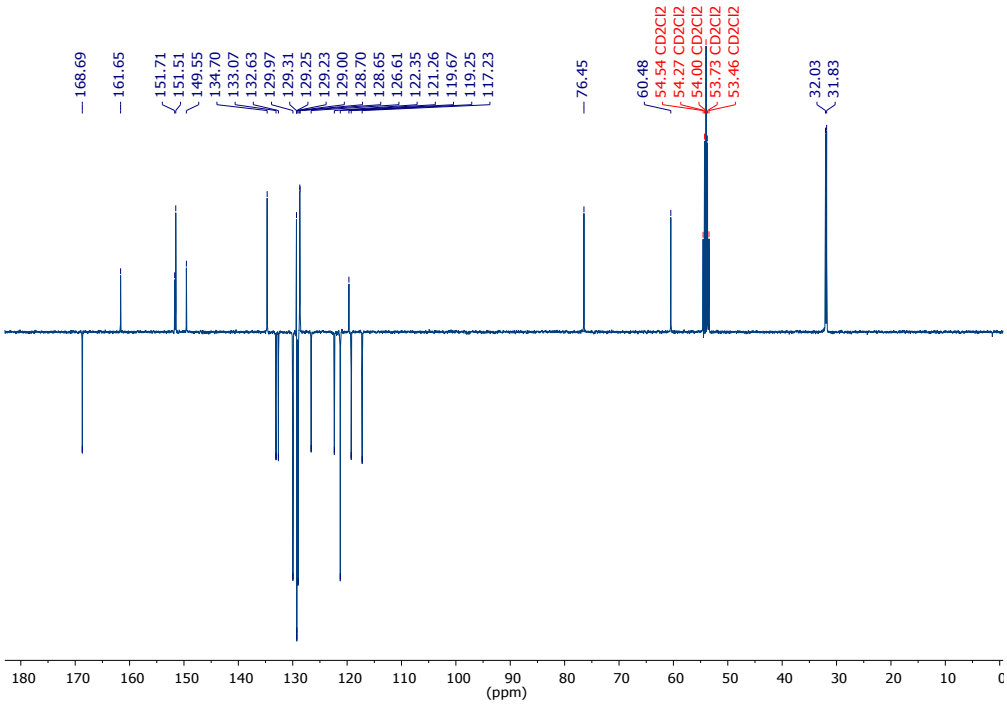

Fig. S14. APT spectrum of **H_4L** in CD_2Cl_2 at ambient temperature.

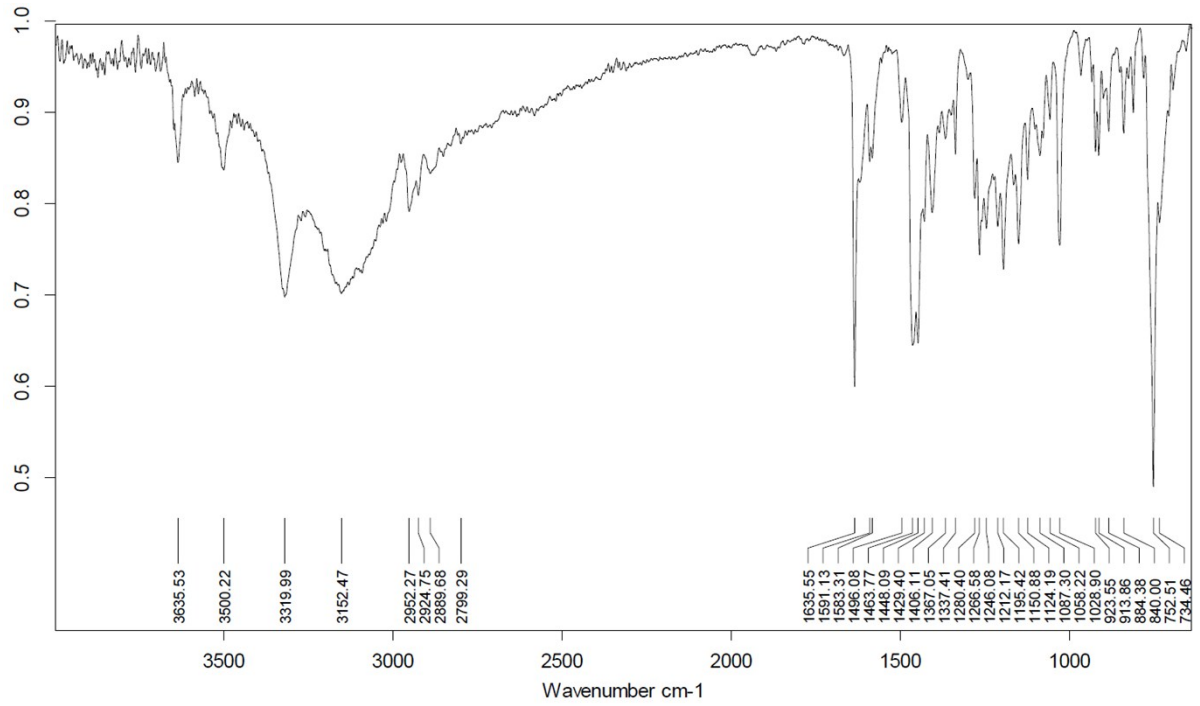

Fig. S15. ATR infrared spectrum of **H_4L**.

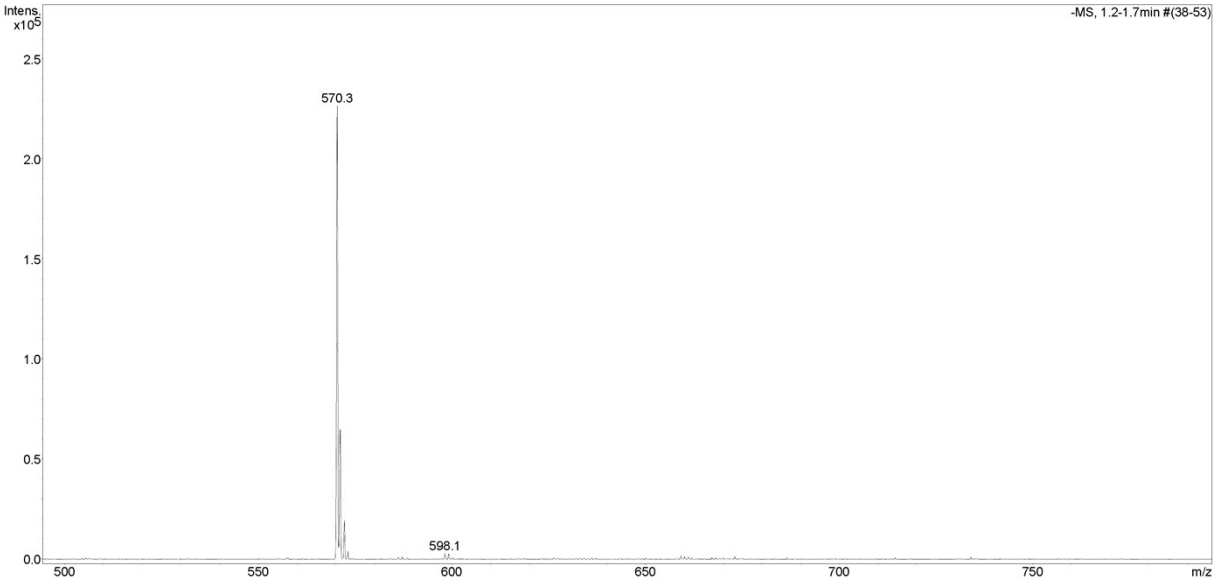

Fig. S16. ESI mass spectrum of **H_4L**.

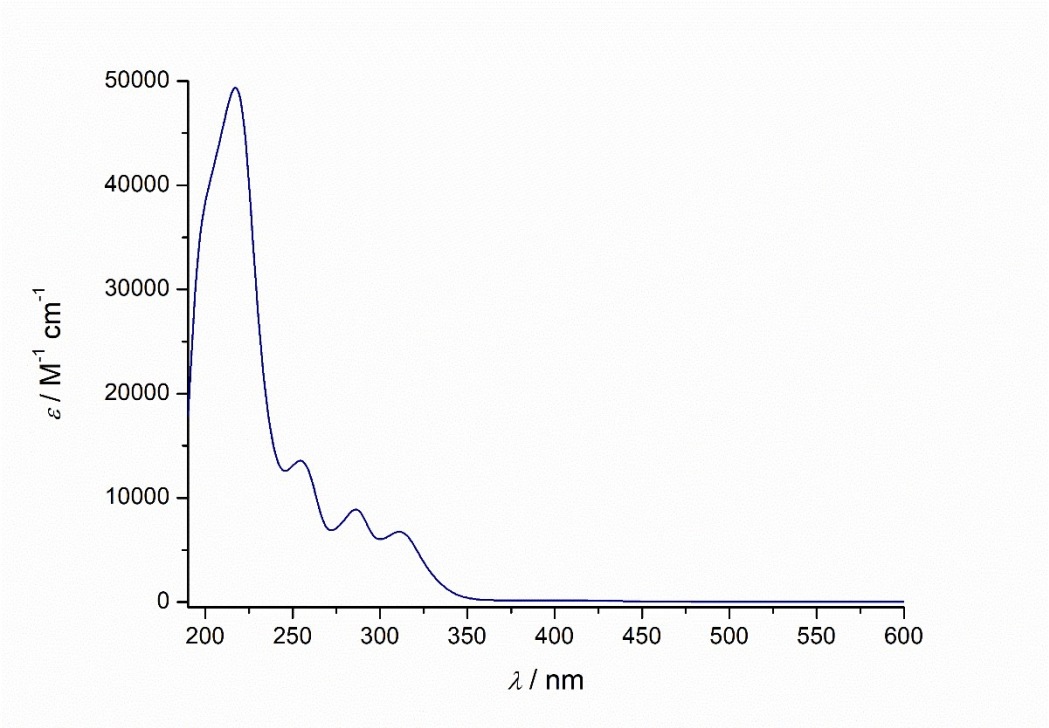

Fig. S17. UV/vis spectrum of **H_4L** in MeCN, [H_4L] = $5 \cdot 10^{-5}$ M.

5. Analytical data for ($NHEt_3$)[Sm_2(L)(HL)] (4)

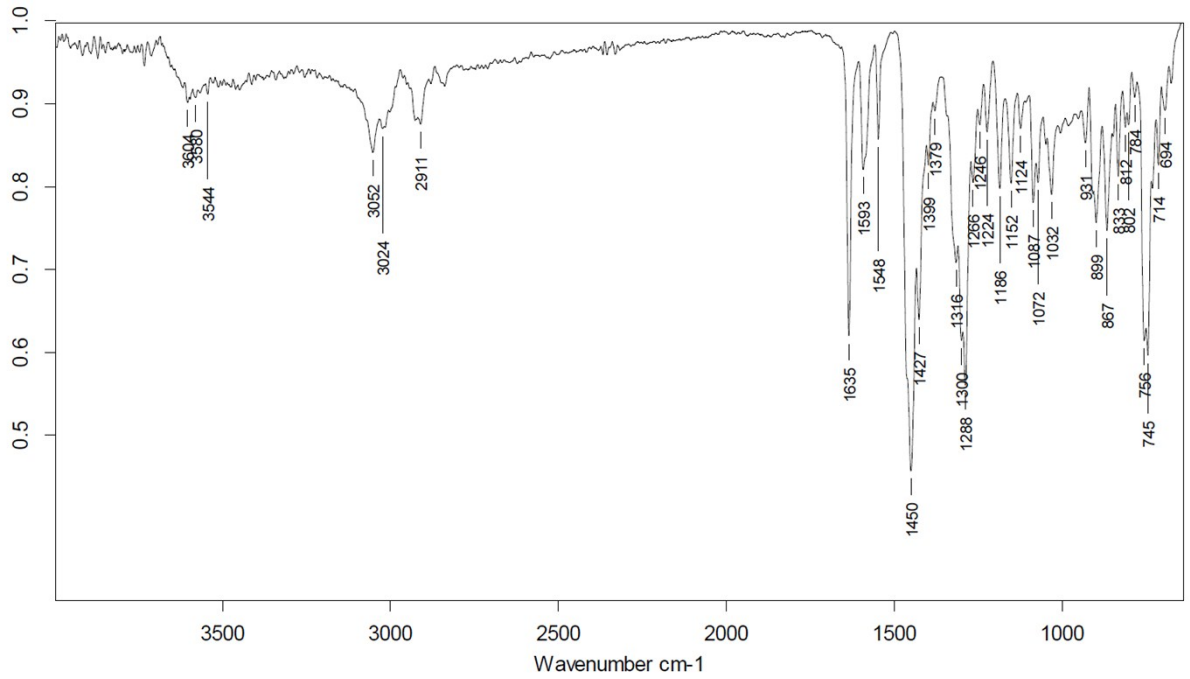

Fig. S18. ATR infrared spectrum of **4**.

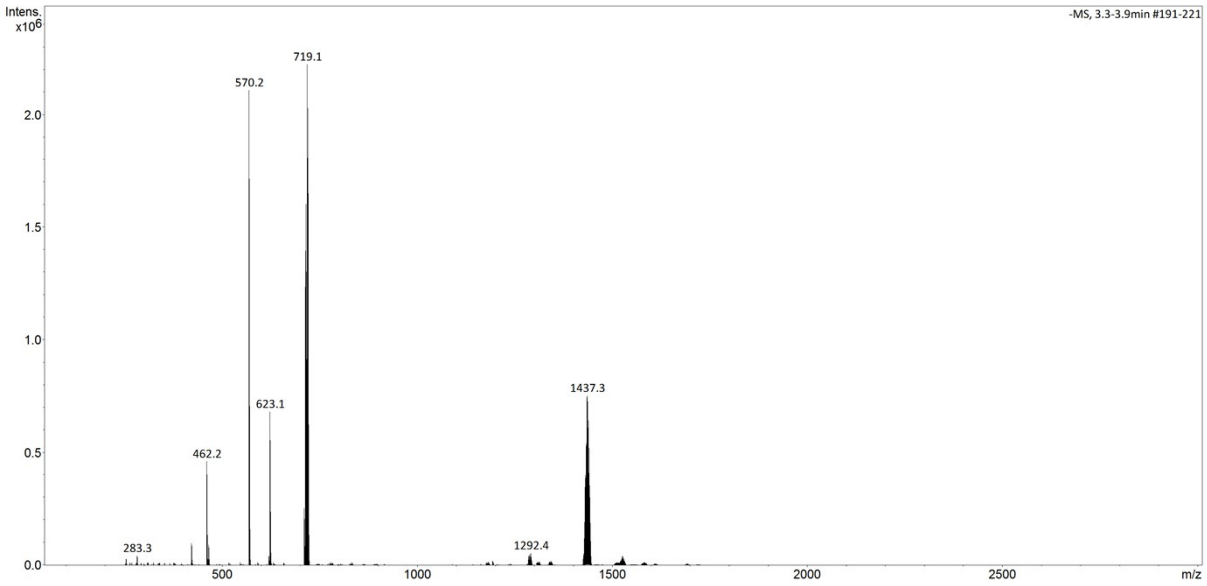

Fig. S19. ESI mass spectrum of **4**.

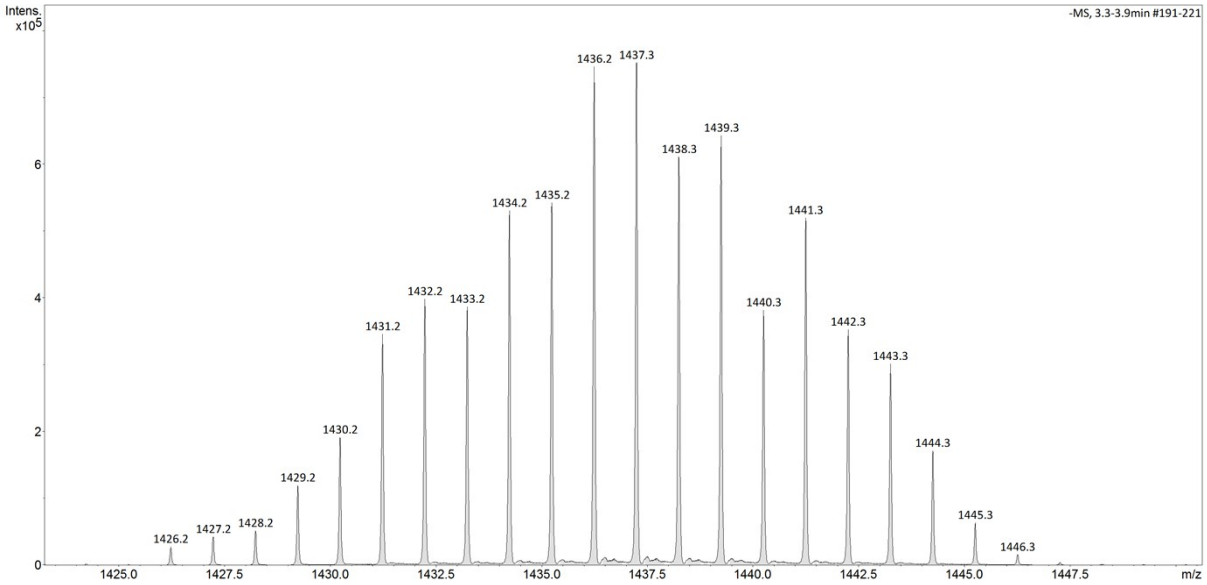

Fig. S20. ESI mass spectrum of **4**.

6. Analytical data for $(NHEt_3)[Eu_2(L)(HL)]$ (5)

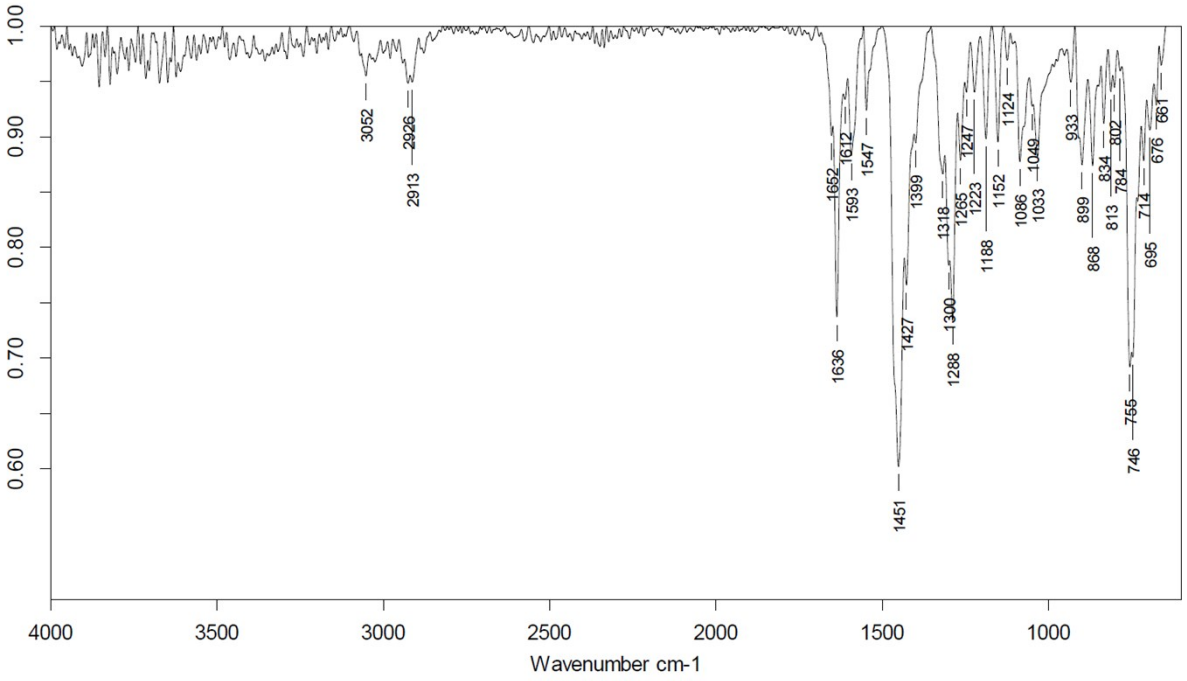

Fig. S21. ATR infrared spectrum of **5**.

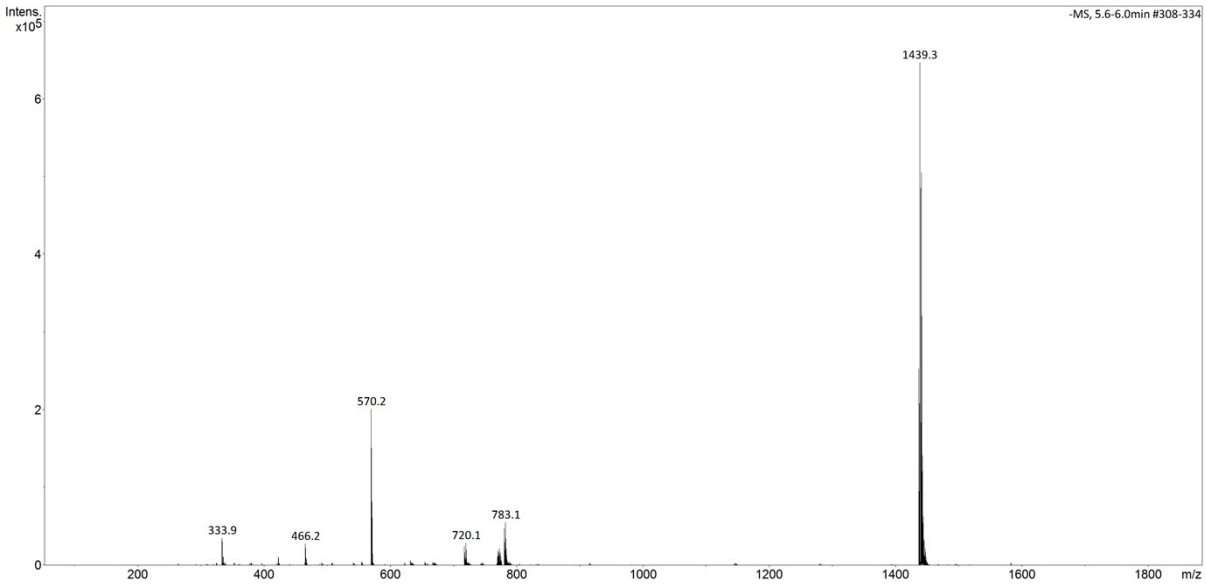

Fig. S22. ESI mass spectrum of **5**.

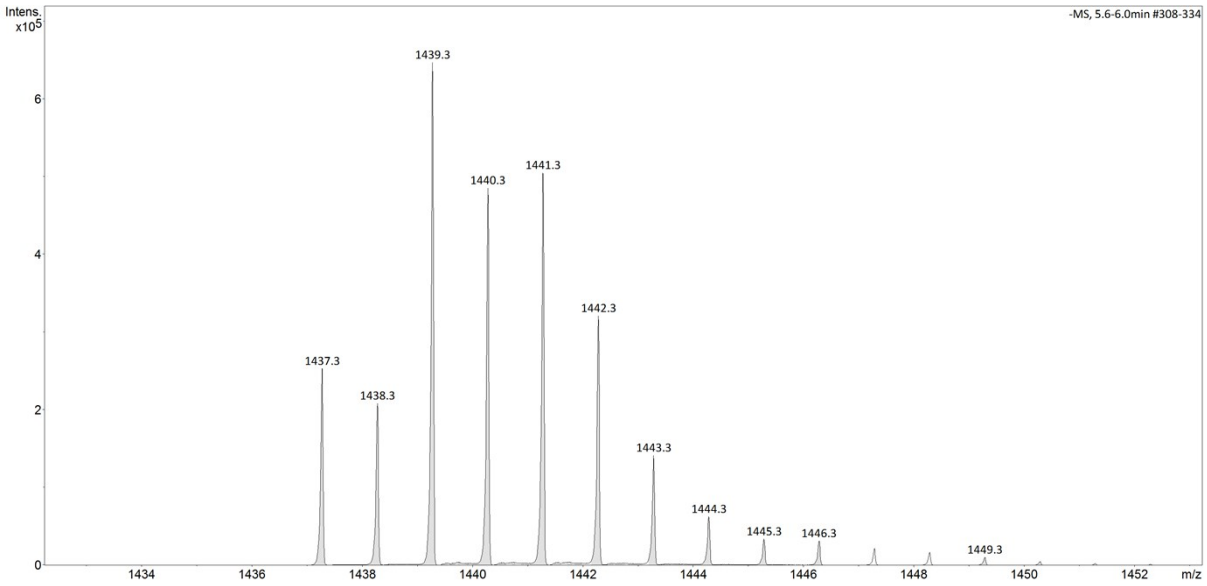

Fig. S23. ESI mass spectrum of **5**.

7. Analytical data for $(HNEt_3)[Gd_2(L)(HL)]$ (6)

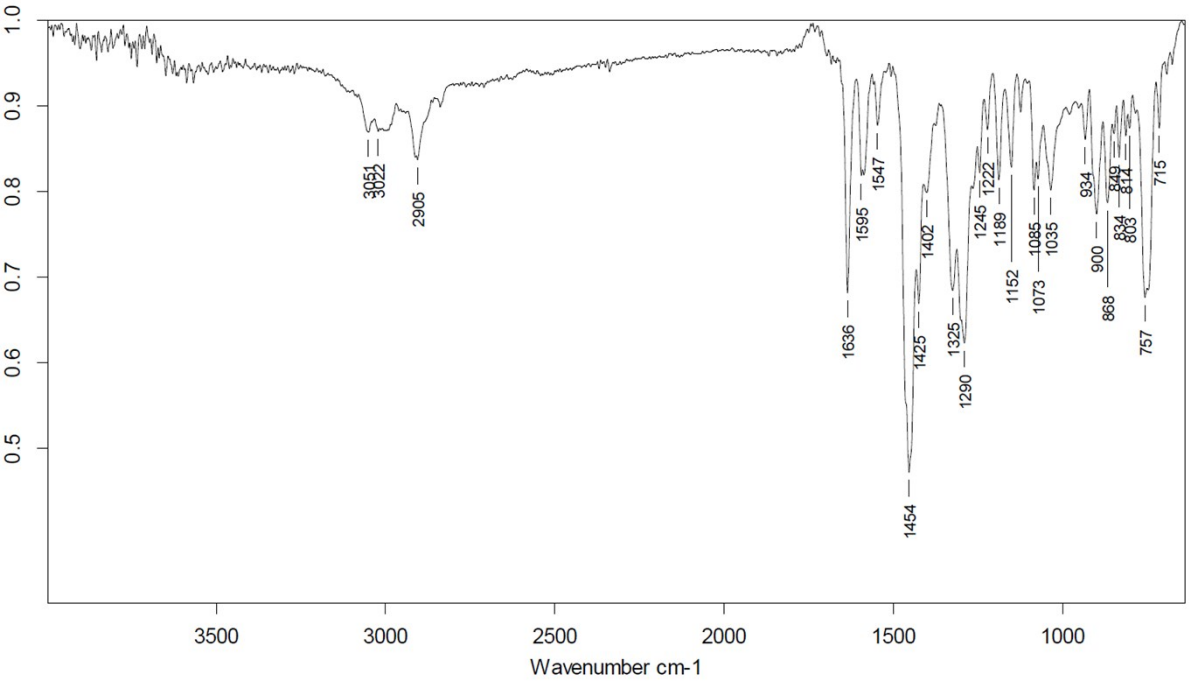

Fig. S24. ATR infrared spectrum of **6**.

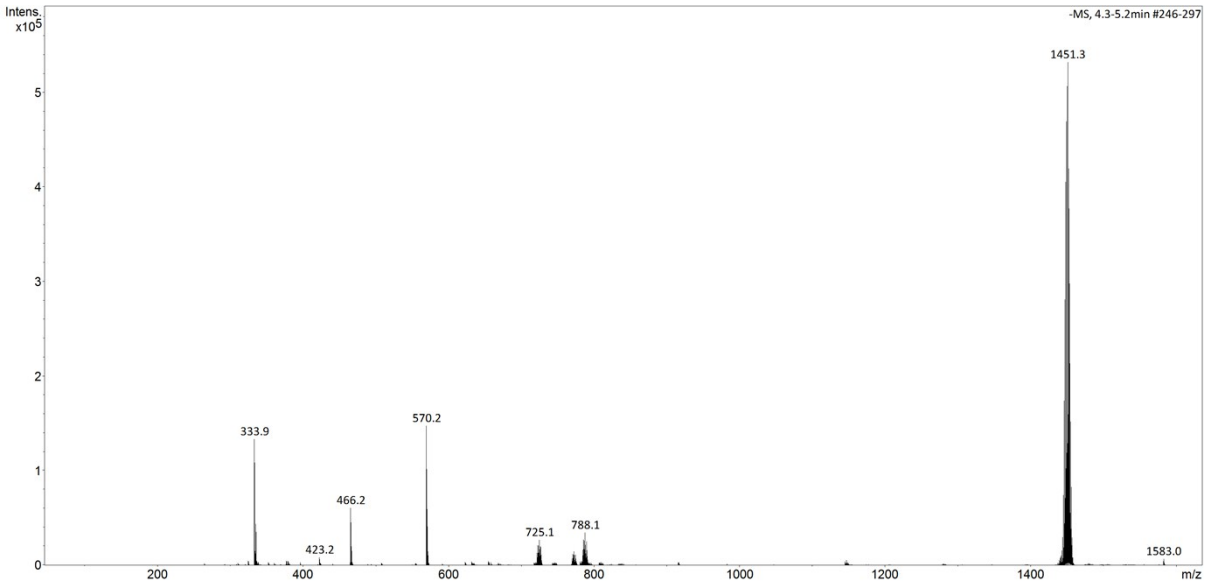

Fig. S25. ESI mass spectrum of **6**.

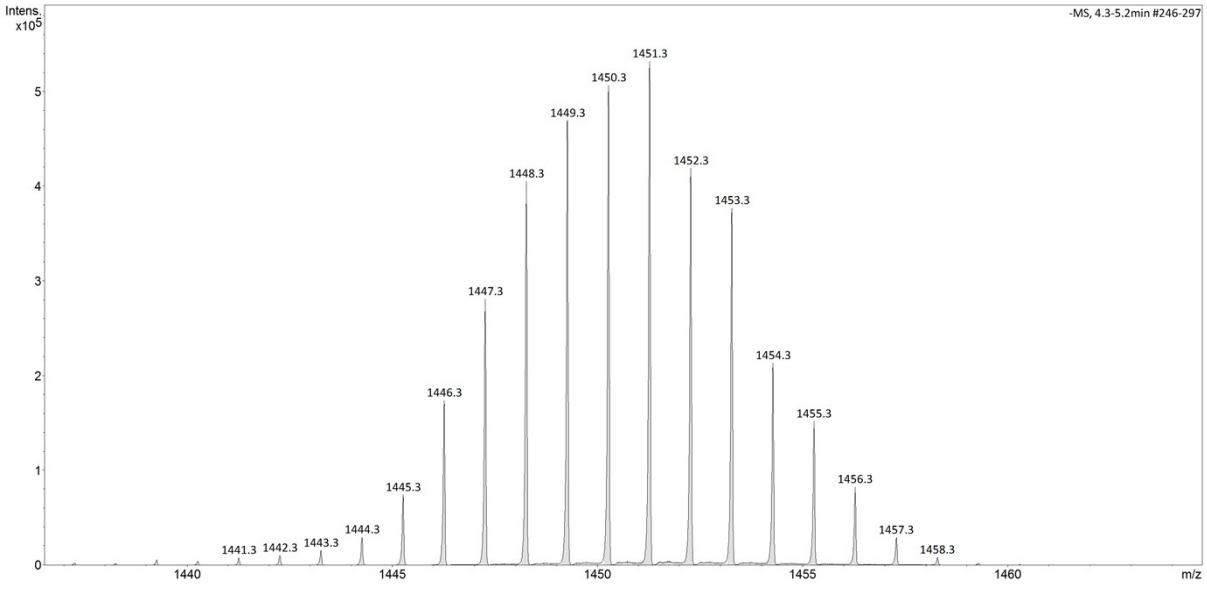

Fig. S26. ESI mass spectrum of **6**.

8. Analytical data for $(HNEt_3)[Tb_2(L)(HL)]$ (7)

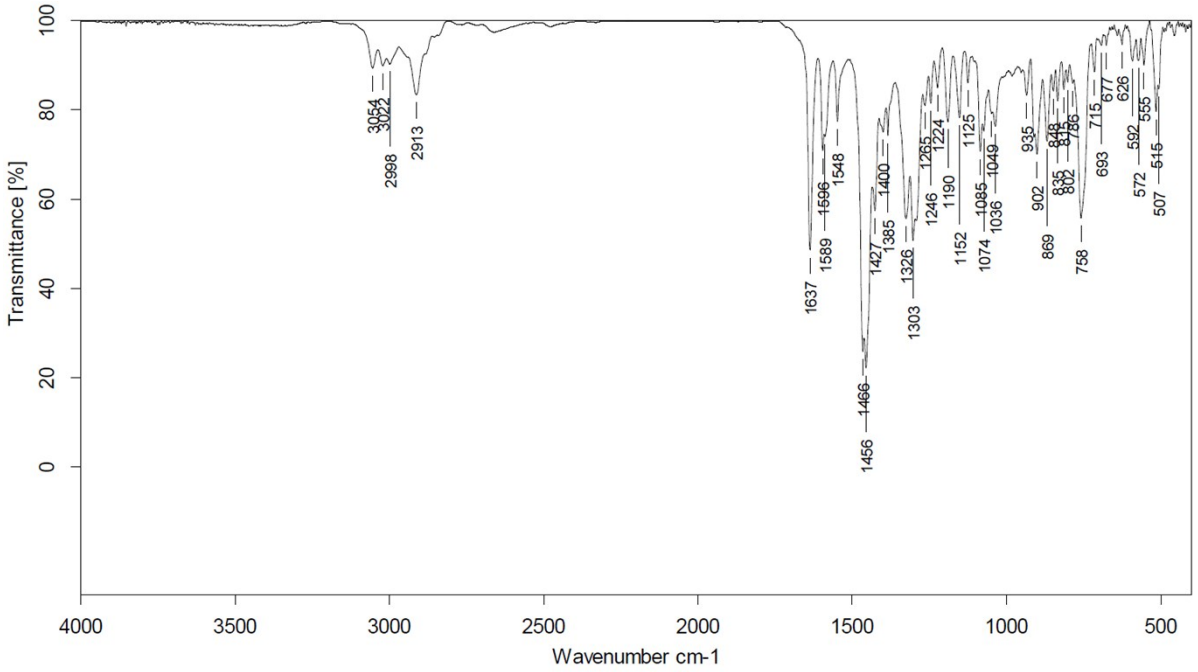

Fig. S27. FT infrared spectrum of **7**.

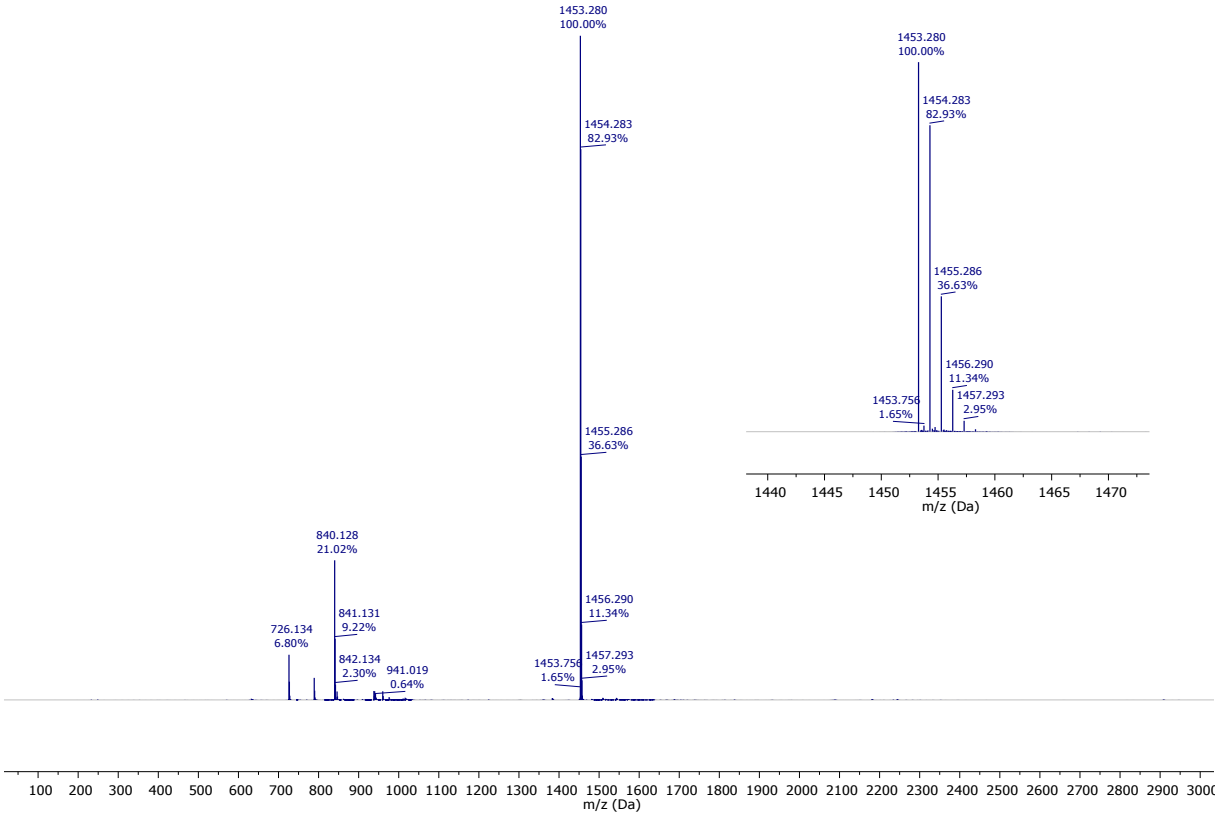

Fig. S28. ESI mass spectrum of **7**.

9. Spectrophotometric titrations / Determination of Stability Constants

Batch data for $(NHEt_3)[Sm_2(L)(HL)]$ (**4**)

HypeSpec refinement output

Project title: Titration of H_4L by $Sm(NO_3)_3 \cdot 6H_2O$

Converged in 1 iteration with sigma = 7,4369E-03

Log beta	value	standard deviation
AB	6.0809	0.0369

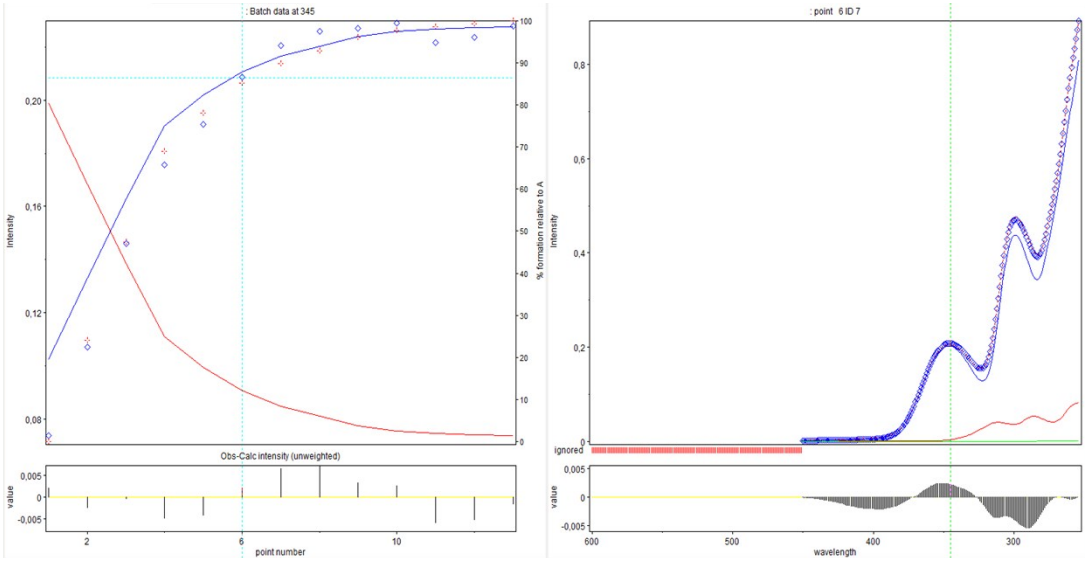

Fig. S29. Titration isotherm extracted at 345 nm (left panel), spectrum corresponding to the 6th data point (right panel), and plot of residuals (bottom panels). Observed absorbance values are plotted as blue diamonds and the calculated ones as red crosses. The solid lines in the right panel show the calculated contribution of H_4L (red), $Sm(NO_3)_3$ (green) and the 1:1 complex (blue) to the total absorbance.

Batch data for $(NHEt_3)[Eu_2(L)(HL)]$ (**5**)

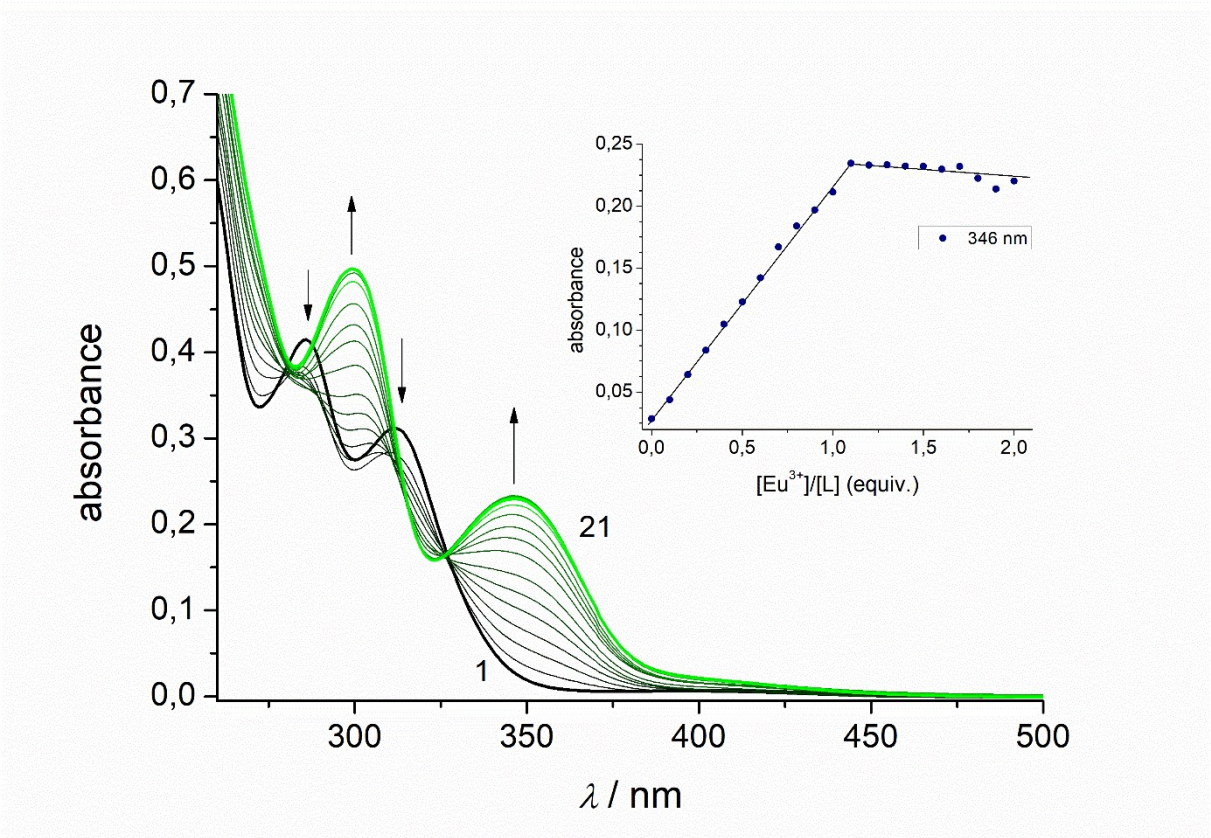

Fig. S30. Spectrophotometric titration of **H_4L** with $Eu(NO_3)_3 \cdot 6H_2O$ in CH_3CN (10^{-5} M concentration) at constant ionic strength (10^{-2} M $N^nBu_4PF_6$, T = 298 K) in the presence of $5 \cdot 10^{-4}$ M NEt_3. The green curve refers to a final molar ratio of M/**H_4L** = 5.0. The inset shows the evolution of selected absorbance values versus the $[Eu^{III}]/[\mathbf{H_4L}]$ molar ratio.

HypeSpec refinement output

```
Project title: Titration of H4L by Eu(NO3)3·6H2O
Converged in 1 iteration with sigma = 0,010570

                    standard
Log beta   value    deviation
AB         6.2137   0.0682
```

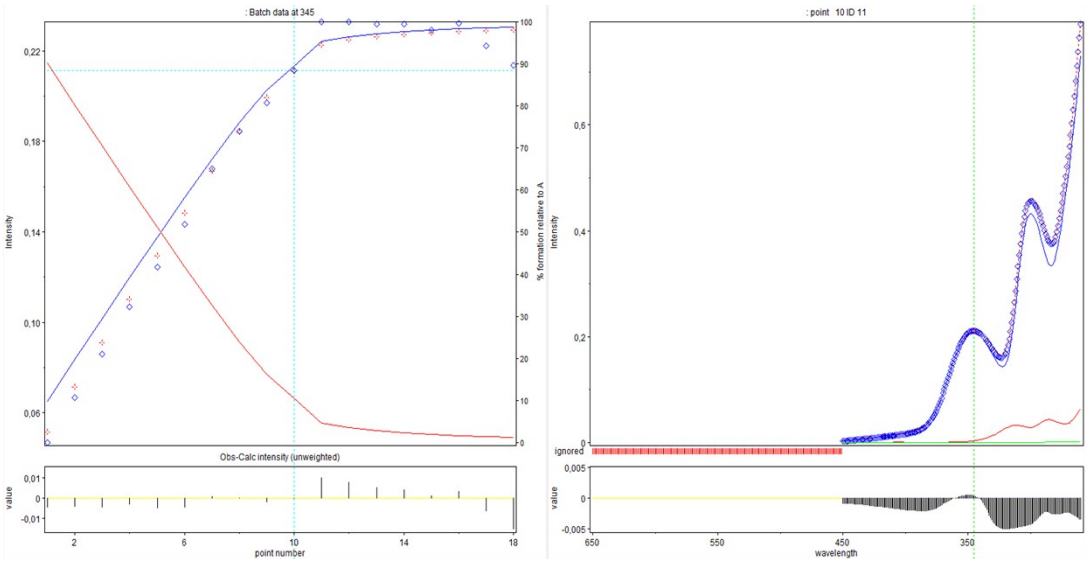

Fig. S31. Titration isotherm extracted at 345 nm (left panel), spectrum corresponding to the 10th data point (right panel), and plot of residuals (bottom panels). Observed absorbance values are plotted as blue diamonds and the calculated ones as red crosses. The solid lines in the right panel show the calculated contribution of H_4L (red), $Eu(NO_3)_3$ (green) and the 1:1 complex (blue) to the total absorbance.

Batch data for $(NHEt_3)[Gd_2(L)(HL)]$ (**6**)

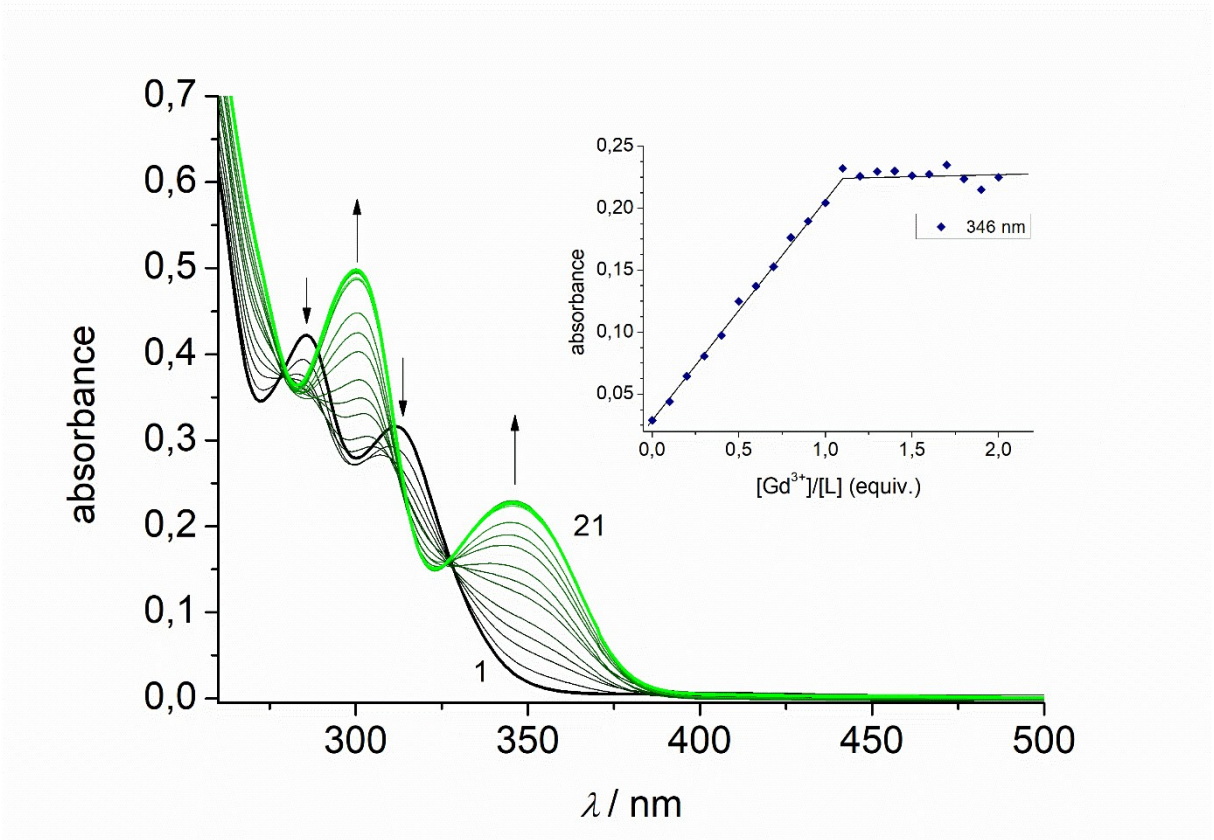

Fig. S32. Spectrophotometric titration of **H_4L** with $Gd(NO_3)_3 \cdot 6H_2O$ in CH_3CN (10^{-5} M concentration) at constant ionic strength (10^{-2} M $N^nBu_4PF_6$, T = 298 K) in the presence of

$5 \cdot 10^{-4}$ M NEt_3. The green curve refers to a final molar ratio of M/**H_4L** = 5.0. The inset shows the evolution of selected absorbance values versus the [Gd^{III}]/[**H_4L**] molar ratio.

HypeSpec refinement output

Project title: Titration of H_4L by $Gd(NO_3)_3 \cdot 6H_2O$
Converged in 1 iteration with sigma = 9,3291E-03

Log beta	value	standard deviation
AB	5.8101	0.043

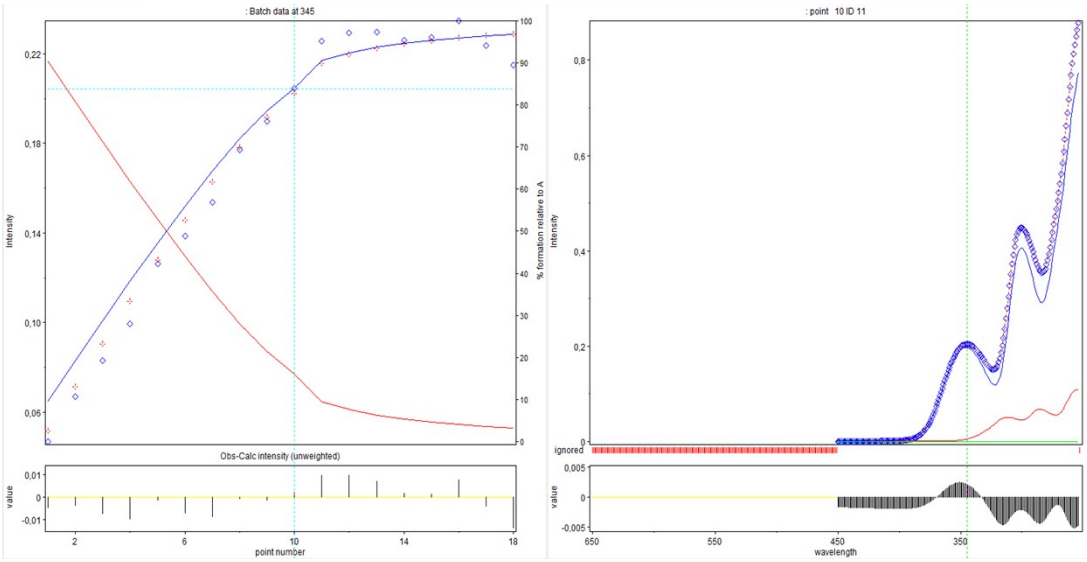

Fig. S33. Titration isotherm extracted at 345 nm (left panel), spectrum corresponding to the 10th data point (right panel), and plot of residuals (bottom panels). Observed absorbance values are plotted as blue diamonds and the calculated ones as red crosses. The solid lines in the right panel show the calculated contribution of H_4L (red), $Gd(NO_3)_3$ (green) and the 1:1 complex (blue) to the total absorbance.

Batch data for $(NHEt_3)[Tb_2(L)(HL)]$ (**7**)

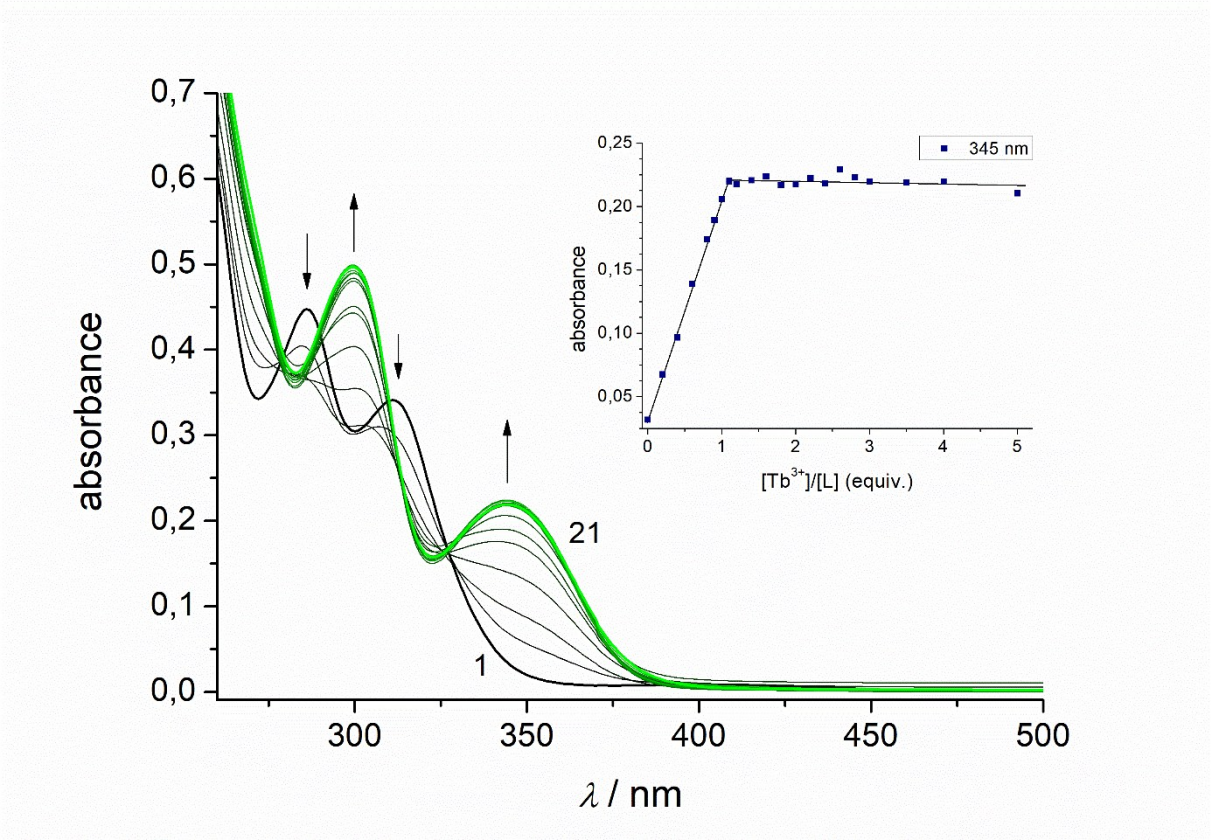

Fig. S34. Spectrophotometric titration of $\mathbf{H_4L}$ with $Tb(NO_3)_3 \cdot 6H_2O$ in CH_3CN (10^{-5} M concentration) at constant ionic strength (10^{-2} M $N^nBu_4PF_6$, T = 298 K) in the presence of $5 \cdot 10^{-4}$ M NEt_3. The green curve refers to a final molar ratio of M/$\mathbf{H_4L}$ = 5.0. The inset shows the evolution of selected absorbance values versus the $[Tb^{III}]/[\mathbf{H_4L}]$ molar ratio.

HypeSpec refinement output

Project title: Titration of H_4L by $Tb(NO_3)_3 \cdot 6H_2O$
Converged in 1 iteration with sigma = 9,0417E-03

Log beta	value	standard deviation
AB	6.3426	0.0604

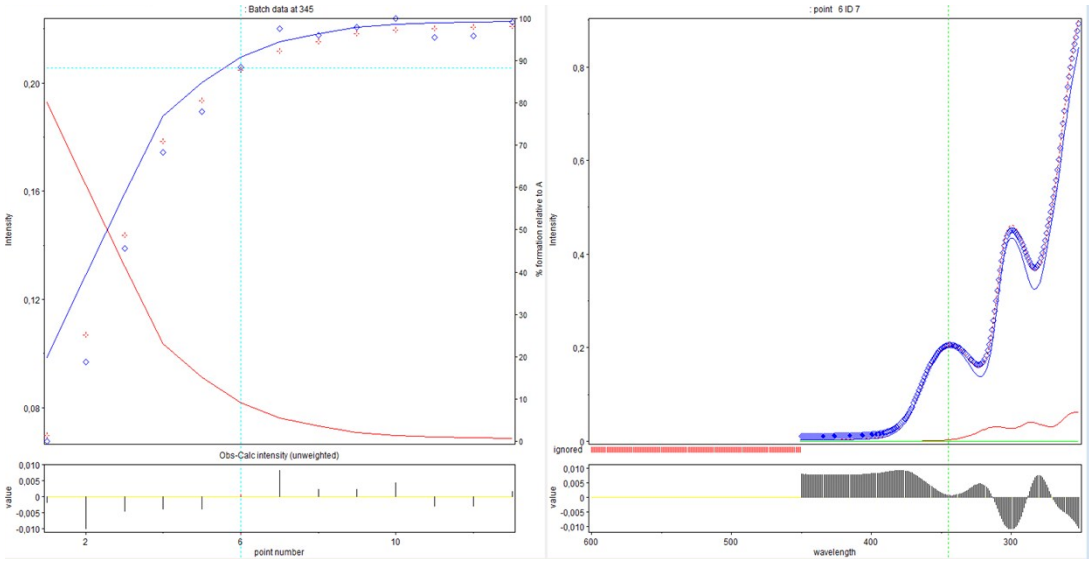

Fig. S35. Titration isotherm extracted at 345 nm (left panel), spectrum corresponding to the 6th data point (right panel), and plot of residuals (bottom panels). Observed absorbance values are plotted as blue diamonds and the calculated ones as red crosses. The solid lines in the right panel show the calculated contribution of H_4L (red), $Tb(NO_3)_3$ (green) and the 1:1 complex (blue) to the total absorbance.

Eq. S1. Expression used for analysis of the temperature dependence of $\chi_M T$ for the dinuclear Sm compound **4**.[1]

$$\chi_M T = \frac{N_a \mu_B{}^2}{3k_B x}(2.143 + 7.347 + (42.92x + 1.641)e^{-7x/2} + (283.7x - 0.6571)e^{-8x} + (620.6x - 1.94)e^{-27x/2} + (1122x - 2.835)e^{-20x} + (1813x - 3.556)e^{-55x/2}) /$$

$$(3 + 4e^{-7x/2} + 5e^{-8x} + 6e^{-27x/2} + 7e^{-20x} + 8e^{-55x/2}) \qquad \text{(S1)}$$

$$x = 1/k_B T$$

Eq. S2: Expression used for analysis of the temperature dependence of $\chi_M T$ for the dinuclear Eu compound **5**.

$$\chi_M T = \frac{N_a \mu_B{}^2}{3k_B x}(24 + (27x/2 - 3/2)e^{-x} + (135x/2 - 5/2)e^{-3x} + (189x - 7/2)e^{-6x} + (405x - 9/2)e^{-10x} + (1485x/2 - 11/2)e^{-15x} + (2457x/2 - 13/2)e^{-21x}) /$$

$$(1 + 3e^{-x} + 5e^{-3x} + 7e^{-6x} + 9e^{-10x} + 11e^{-15x} + 13e^{-21x}) \qquad \text{(S2)}$$

$x = l/k_B T$

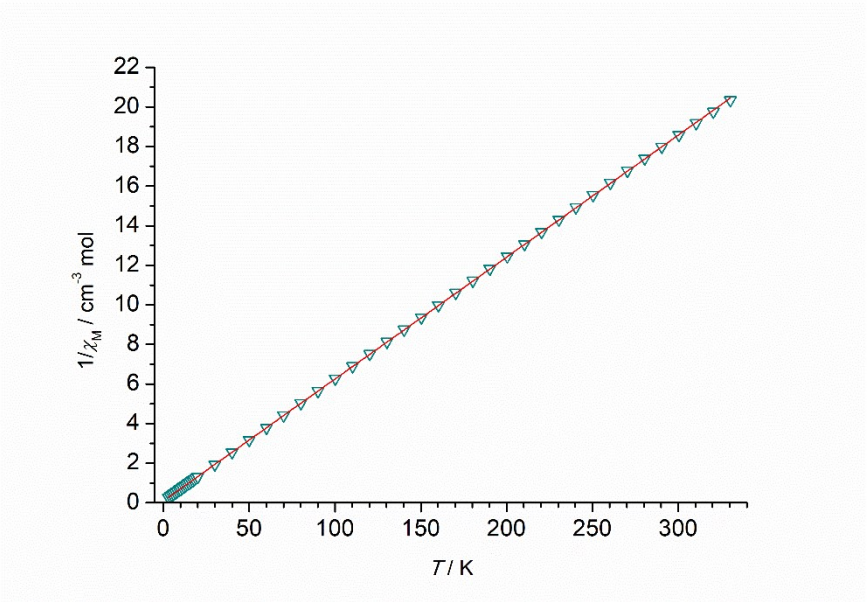

Fig. S36. Temperature dependence of the inverse molar susceptibility (Curie-Weiss plot) of **6**. The solid line corresponds to the best fit of the experimental data.

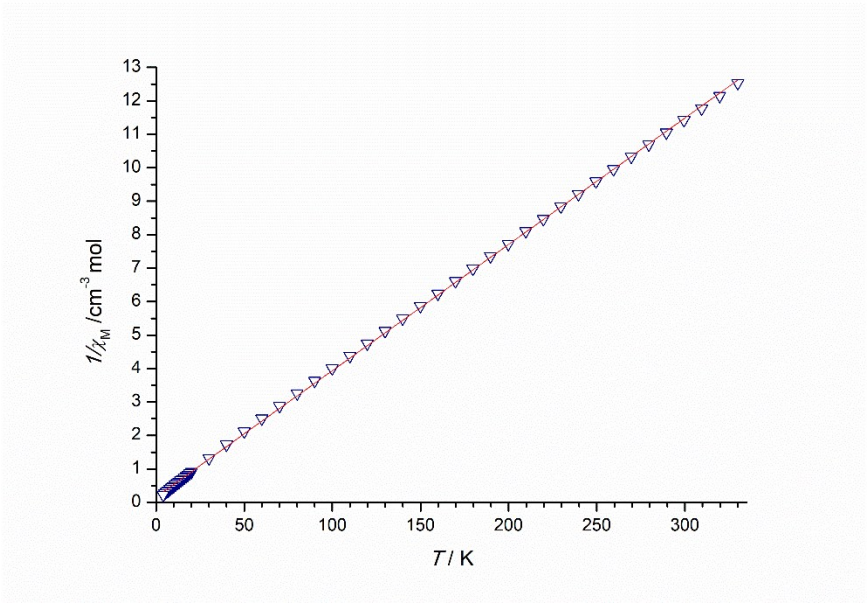

Fig. S37. Temperature dependence of the inverse molar susceptibility (Curie-Weiss plot) of **7**. The solid line corresponds to the best fit of the experimental data.

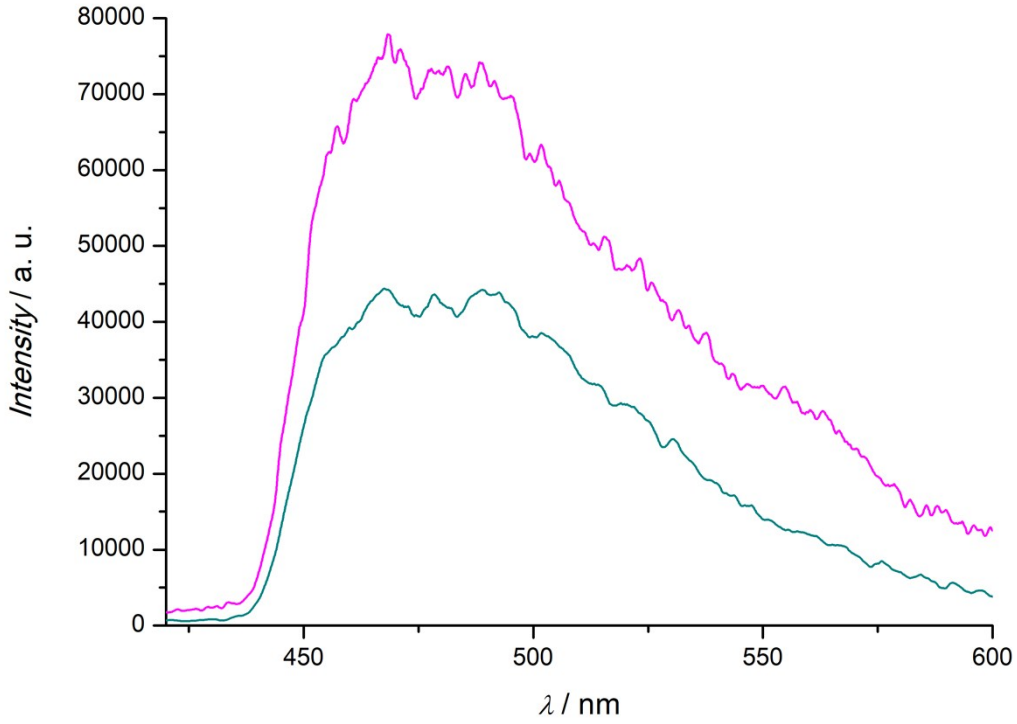

Fig. S38. Emission profile for 4%wt $(HNEt_3)[Gd_2(HL)(L)]$ in polycarbonate matrix at 77 K. Pink: 100 μs delay, dark cyan: 650 μs delay. The excitation wavelength is 285 nm.

---

[1] M. Andruh, E. Bakalbassis, O. Kahn, J.-C. Trombe, P. Porcher, *Inorg. Chem.* **1993**, **32**, 1616-1622.